Chapter 3

Hydrodynamic Vortex Structures in a Diffusion Jet Flame

Dubnishchev Yuri Nikolaevich,
Lemanov Vadim Vladimirovich,
Lukashov Vladimir Vladimirovich,
Arbuzov Vitali Anisiforovich and
Sharov Konstantin Aleksandrovich

Additional information is available at the end of the chapter

http://dx.doi.org/10.5772/intechopen.80610

Abstract

The chapter presents the results of an experimental study of hydrodynamics and diffusion combustion of jets flowing out of long tubes in the Reynolds number range 200–13,500 into air. The methods used in the experiments are visualization in the ultraviolet region, PIV, and hot-wire anemometry. The amplitude-phase structure of optical filters in systems of the Hilbert diagnostics of phase optical density fields in gaseous and condensed systems was used in this work. A possibility of visualization of disturbances in phase optical density fields with arbitrary amplitudes is demonstrated. Two geometries are studied: jet combustion in a stationary atmosphere and in a cross flow. Propane and hydrogen in a mixture with an inert diluent (CO_2) were used as fuels. In the isothermal jet stream, propane-butane mixture and Freon-22 are used. The main attention in the problem is paid to the mechanism of pipe and jet instability interaction, resulting in the vortex motion in several spatial regions. For critical Reynolds numbers in a pipe, the characteristic is the mechanism of two-stage instability caused by turbulent spot (puff) formation inside the pipe and vortex structure generation in the jet-mixing layer. These vortex structures (puff) exert a strong influence both on the isothermal jet and on the flame.

Keywords: jet flame, combustion control, laminar-turbulent transition, vortex structures, turbulence, experiment, visualization

1. Introduction

At present, there are many detailed studies of the jets flowing out of contoured nozzles for turbulent flow regimes (Reynolds number over 5000), where the Kelvin-Helmholtz instability is the key mechanism for the formation of vortices in the initial region [1–3]. The diffusion torch has been also fairly well studied [4]. One of the new and promising methods for controlling combustion is the jet diffusion flame in the regimes of instability evolving both in the jet stream itself and inside the jet source [5–7]. A feature of this problem is the use of jets with low Reynolds numbers, implying low speeds and low mass flow fuel rates. It agrees with the urgent tasks of energy saving and energy efficiency. Such regimes allow obtaining jets with a long laminar zone length. Two-stage instability (inside the jet source and in the jet-mixing layer) may serve as a mechanism controlling the jet flame organization.

The principal difference of this problem statement compared to other works is the mechanism of interaction between instabilities in tube and jet. This leads to the organization of a vortex motion in several spatial regions. At critical Reynolds numbers in a pipe through which fuel is supplied, local organized vortex structures of two types (puff and slugs) are formed [8]. In the jet part of the flame, it is possible to form several vortex zones. A low-frequency flicker instability occurs at the outer boundary of the flame, and the shear instability of the mixing layer can be observed in the core of the torch (in the near-axis zone) [6, 9, 10]. Vortex structures (puff and slugs) formed in transient flow regimes in the tube can have a significant effect on combustion. As shown by our experiments [7], the range of regulation of the flame structure at low Reynolds numbers (Re = 1800–3000) is quite wide. With the help of puff or slugs, it is possible to initiate a transition from a laminar flame to a turbulent one, or vice versa, to realize a laminarization of the reacting flow. As is known, the flowing from the tube (nozzle) can form two types of flame—attached and detached (lifted flame). Using the mechanism of forming vortex perturbations inside the jet source, one can switch the flame from one type to another, and vice versa. And in the case of the action of a vortex disturbance of large amplitude, even a flame blowoff is possible.

The chapter presents the results of an experimental study of jets and diffusion burning of jets by the example of an outflow from a long tube at low Reynolds numbers. Two geometries are studied: jet combustion in a stationary atmosphere and in a transverse airflow. To achieve the goal, the following methods are used: Hilbert visualization, PIV, and hot-wire anemometry. During combustion, propane and hydrogen are used as a fuel in the mixture with an inert gas. Isothermal jets of various gases (propane-butane, CO_2, Freon-22) are also considered. The experiments are carried out when a subsonic gas jet flows into the air space from a tube of 2 and 3.2 mm diameter in the Reynolds number range of 200–15,000. At that, the speed range is 0.3–60 m/s.

2. Optical methods of diagnostics

Optical diagnostics of flows have been successfully applied in experimental hydrodynamics and gas dynamics for a long time. It offers a large variety of modern methods and techniques: shadowgraphy and Schlieren methods [11–13], laser Doppler anemometry [13, 14], Doppler

technologies of velocity field measurements [15, 16], and particle image velocimetry [17]. The Hilbert diagnostics of flows [18–21] based on visualization of space-and-time phase disturbances induced in the light field by the flow passing through the examined medium has a high potential for development and application. Such disturbances are visualized by means of the Hilbert filtration of the optical field, transforming the latter into a Hilbert-conjugate signal.

If the Foucault-Hilbert transform is performed, the result is an analytical signal being superposition of the initial and Hilbert-conjugate fields. The amplitude of these signals contains information about the structure of the phase disturbance.

Though the theoretical and experimental details of the Hilbert optics have been discussed in many publications, its potential is far from being exhausted. This refers, in particular, to the analysis of the amplitude-phase characteristics of the filters and the dynamic range of phase disturbances during the Hilbert diagnostics in the spectral range of the probing field.

The optical measuring complex is based on the serial IAB-463 M shadow device [www.skb-photon] using the optical Hilbert filtering modules, shear interferometry, and light source, specially adapted for the purpose of the experiment. For interferometric studies, a modified shear interferometer is used [18]. **Figure 1** shows a simplified scheme of the experimental setup consisting of an experimental stand and an optical measuring complex. The circuit contains a lighting module consisting of a light source 1, a collimator lens 2, and a slit diaphragm 3. The slit diaphragm is located in the front focal plane of the objective 4, forming a light probe field in the medium under study. The Fourier spectrum of the phase perturbations induced in the medium under investigation is formed by an objective 5 in the frequency plane where a quadrant Hilbert filter 6 is placed. The objective 7 performs the inverse Fourier transformation of the filtered light field, visualizing its phase perturbations, which are recorded by a digital video camera 8 connected to the computer 9.

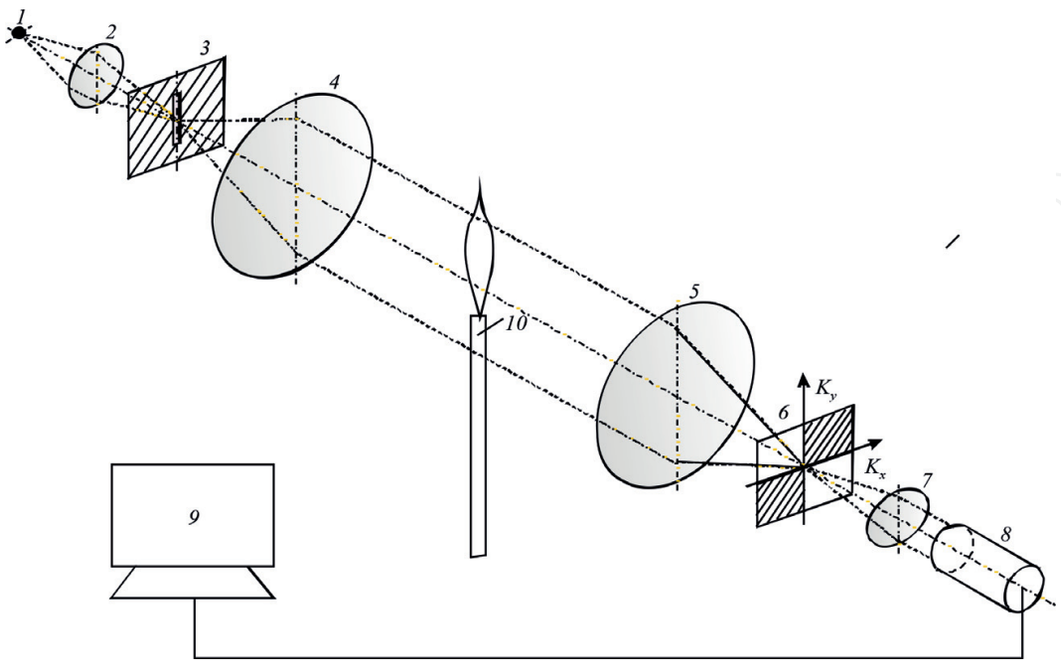

Figure 1. Experimental scheme.

The coherent transfer function of the spatial-frequency filter (HF) performing a one-dimensional Hilbert transform is described by the expression

$$H(K_x, K_y) = \left[e^{-i\varphi}\sigma(K_x) + e^{i\varphi}\sigma(-K_x)\right]\sigma(K_y) + \left[e^{i\varphi}\sigma(K_x) + e^{-i\varphi}\sigma(-K_x)\right]\sigma(-K_y), \tag{1}$$

where K_x and K_y are the spatial frequencies, $\sigma(\pm K_x)$ and $\sigma(\pm K_y)$ are the Heaviside functions, and φ is the phase shift defined by the corresponding quadrant of the spatial-frequency filter. Given that $\sigma(\pm K_x) = \frac{1}{2}[1 \pm \mathrm{sgn}K_x]$, where $\mathrm{sgn}K_x$ is the sign function, expression Eq. (1) for the coherent transfer function of the filter takes the form

$$\begin{aligned} H(K_x, K_y) &= (\cos\varphi - i\sin\varphi \mathrm{sgn}\, K_x)\sigma(K_y) + (\cos\varphi + i\sin\varphi \mathrm{sgn}\, K_x)\sigma(-K_y) \\ &= \cos\varphi - i\left[\sigma(K_y) - \sigma(-K_y)\right]\sin\varphi \mathrm{sgn}\, K_x. \end{aligned} \tag{2}$$

The dynamic representation of the Heaviside functions is used as follows:

$$\sigma(K_y) - \sigma(-K_y) = \int_{-\infty}^{\infty} \sigma(\xi)\delta(K_y - \xi)d\xi - \int_{-\infty}^{\infty} \sigma(\xi)\delta(K_y + \xi)d\xi. \tag{3}$$

Variable ξ is the projection of an arbitrary point of the slit source onto the spatial-frequency axis K_y. This projection has the physical meaning of the zero frequency reference K_x on the spatial-frequency axis K_y. Since $\sigma(\xi) = \frac{1}{2}[1 + \mathrm{sgn}\,\xi]$, expression Eq. (3) takes the form

$$\begin{aligned} \sigma(K_y) - \sigma(-K_y) &= \frac{1}{2}\left\{\int_{-\infty}^{\infty} [1 + \mathrm{sgn}\,\xi]\delta(K_y - \xi)d\xi - \int_{-\infty}^{\infty} [1 - \mathrm{sgn}\,\xi]\delta(K_y + \xi)d\xi\right\} \\ &= \frac{1}{2}\left\{\int_{-\infty}^{\infty} \delta(K_y - \xi)d\xi + \int_{-\infty}^{\infty} \mathrm{sgn}\,\xi\delta(K_y - \xi)d\xi - \int_{-\infty}^{\infty} \delta(K_y + \xi)d\xi + \int_{-\infty}^{\infty} \mathrm{sgn}\,\xi\delta(K_y + \xi)d\xi\right\} \\ &= \frac{1}{2}\left\{1 + \mathrm{sgn}\,K_y + 1 + \mathrm{sgn}(-K_y)\right\} = 1. \end{aligned}$$

Substitution of $\sigma(K_y) - \sigma(-K_y) = 1$ into Eq. (2)

$$H(K_x, K_y) = \cos\varphi - i\sin\varphi \mathrm{sgn}\, K_x. \tag{4}$$

The filter with the coherent transfer function (Eq. (4)) performs a one-dimensional Foucault-Hilbert transform.

In the Fourier plane $H(K_x, K_y)$, the spatial-frequency axis K_x is orthogonal to the image of the slit source. The Fourier spectrum of the light field immediately after the filter has the form

$$s(K_x, K_y)H(K_x, K_y) = s(K_x, K_y)[(\cos\varphi - i\sin\varphi \mathrm{sgn}\, K_x)] = s(K_x, K_y)\cos\varphi + \hat{s}_x(K_x, K_y)\sin\varphi. \tag{5}$$

where $s(K_x, K_y)$ is the spatial-frequency Fourier spectrum of the light field perturbed by the test medium; $\hat{s}_x(K_x, K_y) = -i\mathrm{sgn}(K_x)s(K_x, K_y)$ is the Fourier spectrum of the light field subjected to the one-dimensional Hilbert transform on the K_x axis.

The phase shift φ is a function of the wavelength λ of the probing light field: $\varphi = \varphi(\lambda)$. At a wavelength $\lambda = \lambda_0$ that satisfies the condition $\varphi(\lambda_0) = \pi/2$, the coherent transfer function (Eq. (4)) takes the form

$$H(K_x, K_y) = -i \operatorname{sgn} K_x. \tag{6}$$

In this case, the Fourier filter HF performs a one-dimensional Hilbert transform:

$$\hat{s}_x(K_x, K_y) = -i \operatorname{sgn} K_x s(K_x, K_y). \tag{7}$$

If the investigated medium induces only phase perturbations of the probing field, the Fourier spectrum of the perturbed field is given by

$$s(K_x, K_y) = e^{i\psi(K_x, K_y)}.$$

Accordingly, for the Fourier spectrum of the filtered field, the following is obtained

$$\hat{s}(K_x, K_y) = e^{i\psi(K_x, K_y)} H(K_x, K_y). \tag{8}$$

As follows from Eq. (8), the Fourier spectrum of phase perturbations has a structure consisting of isophase lines satisfying the equation.

$$\psi(K_x, K_y) = \pi m,$$

where $m = 1,\ 2,\ 3\ldots$ and then $\tilde{\psi}(K_x, K_y)$ takes the value of a perturbation of the isophase line that broadens it:

$$\psi = \pi m + \tilde{\psi}(K_x, K_y),\ \tilde{\psi} << 1.$$

In this case, the Fourier spectrum of the light field perturbed by the test medium obtains

$$s(K_x, K_y) = \sum_m e^{i[\pi m + \tilde{\psi}_m(K_x, K_y)]} \approx \sum_m (-1)^m e^{i\tilde{\psi}_m(K_x, K_y)},$$

or taking into account that $\tilde{\psi}_m(K_x, K_y) << 1$,

$$s(K_x, K_y) = \sum_m (-1)^m [1 + i\tilde{\psi}_m(K_x, K_y)]. \tag{9}$$

In view of Eq. (9), the filtered Fourier spectrum of the phase perturbations is expressed as

$$s(K_x, K_y) H(K_x, K_y) = \left\{ \sum_m (-1)^m \left[1 + i\tilde{\psi}_{m_x}(K_x, K_y) \right] \right\} [-i \operatorname{sgn} K_x] = \sum_m (-1)^m \hat{\psi}_{m_x}(K_x, K_y), \tag{10}$$

where $\hat{\psi}_{m_x}(K_x, K_y)$ is the Fourier spectrum of the phase perturbations visualized by means of the Hilbert transform on the x axis. As follows from Eq. (10), phase structures are visualized by

Hilbert filtering. Here, it is taken into account that the Hilbert image of constant quantities is zero according to the properties of the Hilbert transform.

The camcorder lens $L4$ performs an inverse Fourier transform of the filtered Fourier spectrum of phase perturbations:

$$\sum_m \hat{\psi}_{m_x}(K_x, K_y) \leftrightarrow \sum_m \hat{\psi}_{m_x}(x, y). \tag{11}$$

The phase structures Eq. (11) visualized by the one-dimensional Hilbert transform operation are recorded by the camcorder CCD array:

$$\left| \sum_m \hat{\psi}_{m_x}(x, y) \right|^2 = \sum_m \left| \hat{\psi}_{m_x}(x, y) \right|^2. \tag{12}$$

Suppose that white light filtering is performed, the test medium is dispersionless, and the Fourier spectra are achromatic. The quadrature-phase filter performing a Hilbert transform at the wavelength λ_0 is used for filtering in the wavelength range (λ_1, λ_2):

$$H(K_x, K_y) = \cos\varphi(\lambda) - i \sin\varphi(\lambda) \operatorname{sgn} K_x. \tag{13}$$

Integrating the filtered Fourier spectrum in the wavelength range (λ_1, λ_2)

$$\int_{\lambda_2}^{\lambda_2} s(K_x, K_y) H(K_x, K_y) d\lambda \approx s(K_x, K_y) \int_{\lambda_1}^{\lambda_2} H(K_x, K_y) d\lambda. \tag{14}$$

When using a white light source, the weight coefficients $\cos\varphi(\lambda)$ and $\sin\varphi(\lambda)$ (13) are transformed into

$$\int_{\lambda_1}^{\lambda_2} \cos\left(\frac{\pi}{2}\frac{\lambda}{\lambda_0}\right) d\lambda = \frac{4\lambda_0}{\pi} \cos\left[\frac{\pi}{4\lambda_0}(\lambda_2 + \lambda_1)\right] \sin\left[\frac{\pi}{4\lambda_0}(\lambda_2 - \lambda_1)\right]. \tag{15}$$

$$\int_{\lambda_1}^{\lambda_2} \sin\left(\frac{\pi}{2}\frac{\lambda}{\lambda_0}\right) d\lambda = \frac{4\lambda_0}{\pi} \sin\left[\frac{\pi}{4\lambda_0}(\lambda_1 + \lambda_2)\right] \sin\left[\frac{\pi}{4\lambda_0}(\lambda_1 - \lambda_2)\right]. \tag{16}$$

Hence we obtain the partial ratio of the Hilbert image to the original signal:

$$\frac{\int_{\lambda_1}^{\lambda_2} \sin(\lambda) d\lambda}{\int_{\lambda_1}^{\lambda_2} \cos(\lambda) d\lambda} = \operatorname{tg}\left[\frac{\pi}{4\lambda_0}(\lambda_1 + \lambda_2)\right] = \operatorname{tg}\left(\frac{\pi}{2} + \frac{\pi\Delta\lambda}{4\lambda_0}\right) = \operatorname{ctg}\left(\frac{\pi\Delta\lambda}{4\lambda_0}\right). \tag{17}$$

The weight coefficients $\cos\varphi(\lambda)$ and $\sin\varphi(\lambda)$ of the signal and a Hilbert-conjugate signal in the spectral band are equal: $\Delta\lambda = \lambda_1 - \lambda_2$. For $\Delta\lambda \to 0$, a pure Hilbert transform occurs. The

Hilbert transform has quasi-differentiation properties. Therefore, the extreme of the phase distribution and the region of the maximum phase gradient region are transformed into Hilbert ranges.

3. Experimental equipment

The first one studied in the work was the jet without combustion ("cold jet") and then the jet under combustion conditions ("hot jet"). In "cold" experiments, propane-butane mixture (50% propane and 50% butane) and Freon-22 (CHF_2Cl) were used as a working gas. In the experiments with flame, propane and hydrogen were used both in pure forms (Y = 99.9% by volume) and in the mixture with inert diluent (CO_2). The flow in the experiments had atmospheric pressure and the initial room temperature. The equipment included gas vessels, gas reducers, and two flowmeters (**Figure 2**). The gas flow rate and the composition of the fuel mixture were set using digital flowmeters El-Flow Bronkhorst. The viscosity of the gas mixture necessary for calculations was estimated using the Sutherland model in the Wilke approximation [22].

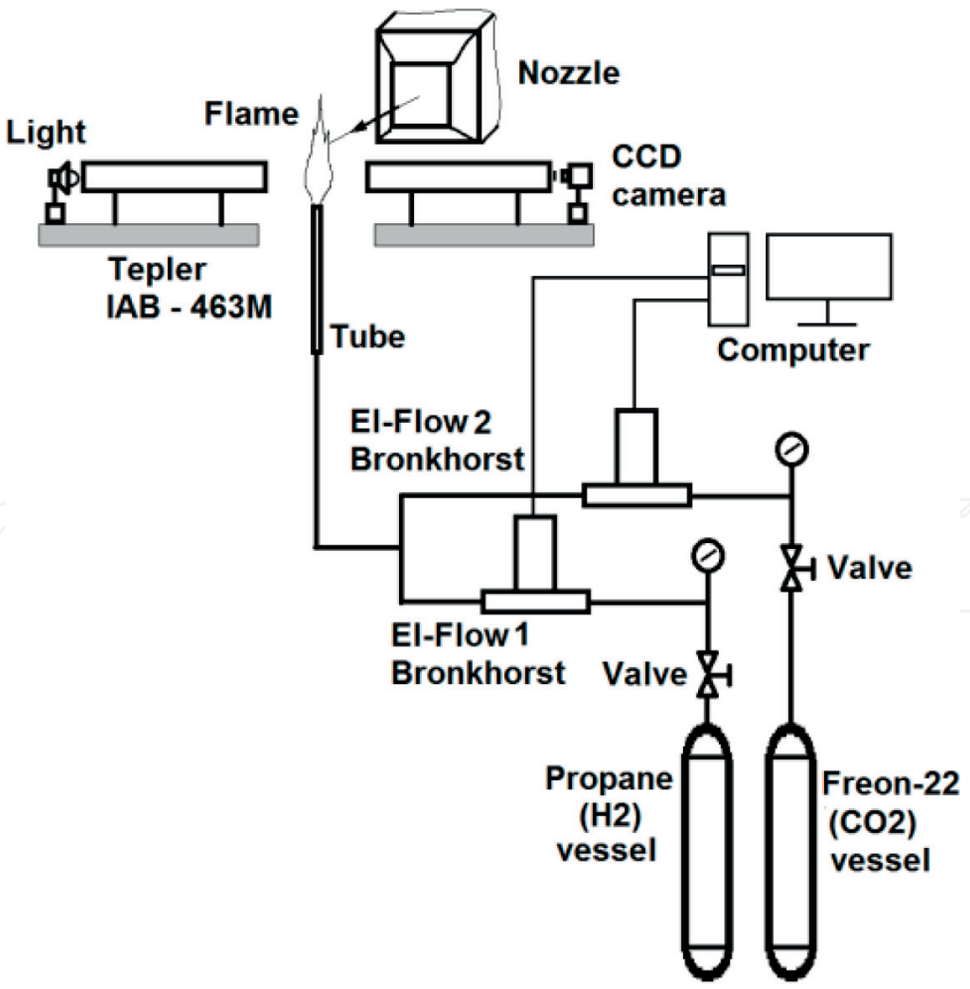

Figure 2. Scheme of setup.

Figure 2 shows a simplified scheme of the experimental setup with a complex for optical diagnostics. The registration of the shift interferograms and the video recording of the torch were made by a digital camera Canon 650D with a frequency of 50 fps. In addition, the high-speed visualization of light-scattering particles placed in the stream illuminated with a laser sheet was carried out with a Photron SA5 camera (4 kHz, the volume of one sample was 11,000 frames). The dynamic characteristics were measured by a constant temperature hot-wire anemometer DISA 55 M. To study the jet in a cross flow, a 2D PIV system was used; it is consisting of a digital camera with a 4 MPix matrix, a pulse laser with pulse energy of 90 mJ, a synchronizer, and a computer. To photograph the chemiluminescence of the OH radical (ultra-violet range), the DiCAM-PRO camera was used. Round tubes of quartz glass were used as a jet source (with an internal diameter d = 3.2 mm with a length L = 550 mm and d = 2 mm with a length L = 1000 mm). The transverse airflow was created with the help of an aerodynamic setup that allowed setting the speed at 1.5–15 m/s in the working part with a cross section of 100 × 100 mm.

4. Free jet investigation

At the first stage, experiments were performed in a "cold jet." It is known that the jet flow dynamics is significantly influenced by the initial conditions [1–3]. **Figure 3a** shows the dependence of the axial mean velocity (U_0) and the root-mean-square value of velocity pulsations (u) on the axis in the tube outlet cross-section as a function of the Reynolds number of the jet ($Re = d \cdot U_m/\nu$, where U_m is the bulk velocity). **Figure 3b** presents the dependence of the turbulence degree ($Tu = u/U_0 \times 100\%$) on Re. As can be seen from **Figure 3**, for the dependence of the average velocity on the Reynolds number, there is a local decrease in U_0 in the region of Re = 1800–2000. The experiments have shown that in this range of Re numbers, the velocity profile is changed from the laminar Poiseuille distribution to the fully developed turbulent profile.

For the root mean square value of the velocity pulsations u and the turbulence degree Tu, a local extremum is observed in the transition region at Re = 1920, and the maximum value of the

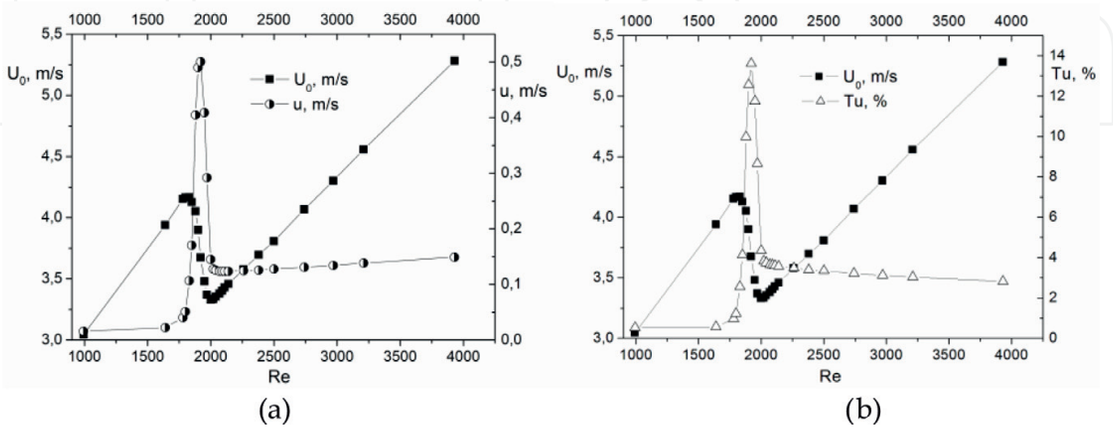

Figure 3. Parameters in the initial section on the axis of the "cold" jet (propane-butane) d = 3.2 mm and l = 500 mm: (a) the mean velocity and rms of the longitudinal velocity pulsations and (b) the mean velocity and degree of turbulence.

turbulence degree Tu = 13.5% is reached. The study of the oscillograms of the hot-wire anemometer signal at the tube outlet has shown the intermittent character of the instantaneous velocity behavior with respect to time and the presence of turbulent spots (puff) in the region of Reynolds transition numbers δ·Re/Re = 7–8%. At Re > 2100, the character of the oscillograms becomes completely turbulent. Thus, the obtained data indicate the presence of a laminar-turbulent transition at the outlet from the tube in the region of Re = 1800–2000 for the propane-butane mixture [8].

Further measurements were made by a hot-wire anemometer on the axis of the gas jet downstream. **Figure 4a** shows the dependence of the velocity on the jet axis U_x, normalized to the initial velocity U_0, on the dimensionless distance x/d for the Reynolds number variation (x is the longitudinal coordinate with its beginning at the start of the jet). The general character of the velocity variation along the axis is a monotonic decrease in the relative velocity U_x/U_0. As can be seen from **Figure 4**, the major changes of the velocity distribution along the axis occur in the region of Reynolds numbers characteristic for the laminar-turbulent transition Re = 1800–1915. At Re = 1820, the longest laminar flow zone is observed.

The change in the rms value of velocity pulsations and the degree of turbulence as a function of the Reynolds number on the jet axis are shown in **Figure 4b**. Here, several characteristic modes of the jet propagation can be distinguished. The instability waves in the mixing layer (basically, an asymmetric mode) were observed at Re > 200. For jets with small Reynolds numbers (Re = 500), an extended laminar flow zone with a low level of velocity pulsations is a characteristic. After that a laminar-turbulent transition region with an increase in pulsations (up to x/d = 20) takes place.

The next region is a zone of turbulent flow where pulsations decrease. With an increase in the Reynolds number, the length of the laminar part decreases, and the maximum of pulsations in the transition region increases. At Re = 1820, the length of the laminar zone is x/d = 10, and the pulsations level reaches Tu = 21%. At Re = 1915, there is a sharp increase in the level of velocity pulsations in the initial section of the jet. In the oscillogram of the hot-wire anemometer signal, an intermittent character of the behavior of instantaneous velocity with the presence of turbulent

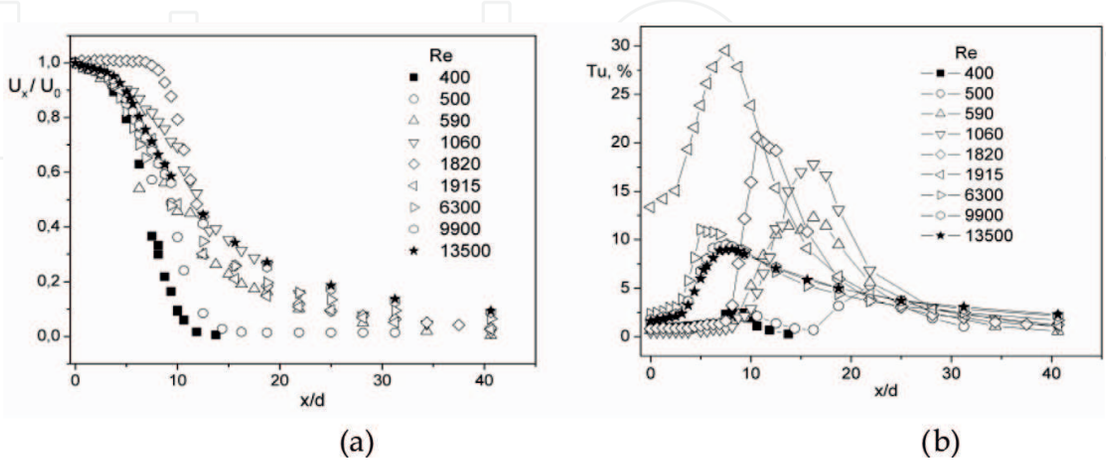

Figure 4. Dynamic parameters along the jet axis with varying Re number, d = 3.2 mm L = 500 mm: (a) dimensionless mean velocity and (b) the degree of turbulence.

spots is observed. The above observations indicate that the laminar-turbulent transition occurs already inside the source of the jet (tube). As a result, the fluctuations in the near field of the jet increase sharply (at x/d = 7 to Tu = 30%). With a further increase in the Reynolds number (Re > 1915), the initial level of pulsations decreases to Tu_0 = 4%, and the maximum at x/d = 7 decreases to the value Tu = 12%. Further downstream (x/d > 7), there is a significant decrease in pulsations, which indicates a strong dissipation of turbulent energy.

Previously, experimental studies of the hydrodynamics of subsonic gas jets in the Reynolds number range 200–4000 have been carried out. One of the important issues is the length of the laminar part of the jet. Our research shows that it can be 100–250 d [23–25]. This task is promising from the point of view of the formation of a long-length flame and requires further study. In the "laminar" regime, when there is no puff, the instability of the jet flow prevails [2, 3], which allows controlling the vortex structures, for example, by acoustic action. The use of a denser gas as a working fluid makes it possible, due to the density gradient, to weaken the effect of this instability [26] and increase the length of the laminar part of the jet. Thus, it becomes possible to observe the development of a vortex structure in the jet stream.

The characteristic times for the existence of unstable flow regimes are characterized by the data presented in **Figure 5**. The experimental conditions correspond to **Figure 4b**; the sample was 11,000 frames; and the shooting frequency was 4 kHz. The observation time of the hydrodynamic disturbance in the field of the frame in the near field of the jet (x/d < 6) was taken as an event. The histogram of the vortex structure lifetime is distributed over time with a lag of 0.01 s. The ordinate represents the number of events in a given interval.

It can be seen that short events (the example is shown in **Figure 5a**) occur rarely (the first from the left quantile in **Figure 6**). Long-term events are also fixed quite seldom (the first from the

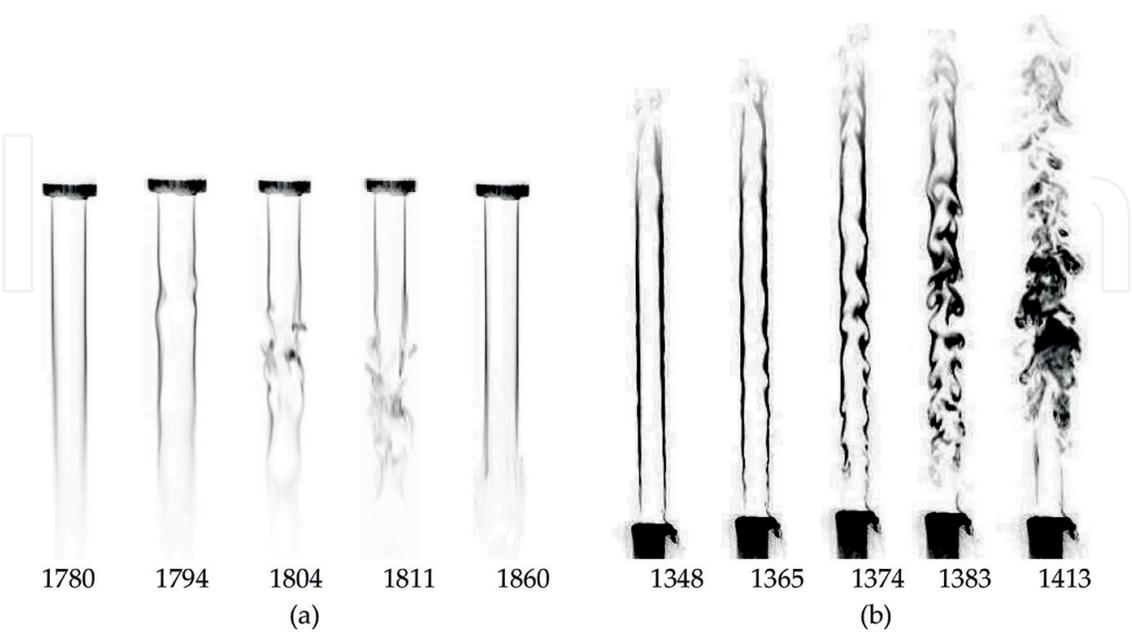

Figure 5. Expansion of the Freon-22 jet top-down (a) into the stationary air at Re = 1740 (see Video 1) and bottom-up (b) into the stationary air at Re = 2230 (Video 2).

http://dx.doi.org/10.5772/intechopen.80610

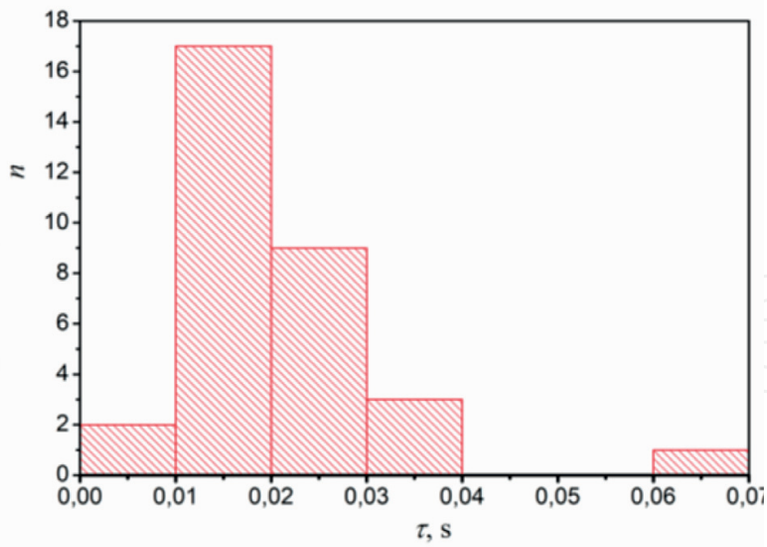

Figure 6. Histogram of the turbulent vortex structure distribution.

right quantile in **Figure 5**). The average time of the perturbation was 0.018 s (e.g., see **Figure 5b**). If the bulk velocity in the tube U_m is taken as a characteristic, then the estimate of the spatial scale of the jet instability in the near field gives the value L/d = 13.7. This value is close to the estimates of the extent of the turbulent spot inside the tube obtained by direct numerical simulation [26]. The question of the spatial vortex structure of such perturbations inside the tube is considered, for example, in [27, 28]. They represent a system of longitudinal vortices. Their arrangement in the cross section of the pipe has symmetry in the azimuth direction (a total of eight vortices). The presented investigations have shown (see **Figure 5**) that a turbulent spot in the initial part of the jet has a more complex vortex structure and requires additional studies.

A two-cascade instability mechanism is established in the work. The first cascade is a mode with intermittency inside the tube (alternation of the turbulent spots and laminar zones at the exit from the tube). The second cascade is the canonical instability of the jet-mixing layer. The study of the interaction of puff with large-scale structures of the mixing layer is the further task. This mechanism gives the prospect for controlling the flame by forming turbulent spots inside the pipe and vortex structures in the jet.

5. Investigating the diffusion jet flame

Quite many studies focus on the diffusion jet flame [4]. In this part of the paper, the main attention is paid to the interaction of vortex structures (puff), formed as a result of a laminar-turbulent transition in a long tube, with the jet flame. In this case, variants of the attached and lifted flame, as well as its extinction, are shown. The Reynolds number of the tube flow transition is conservative to the composition of the fuel mixture. However, the scenario diversity (very sensitive to the fuel mixture composition) of the flame-vortex interaction fundamentally distinguishes combustion from isothermal flow.

The main method of investigation in this part is Hilbert visualization. Diffusion combustion of a jet of a fuel mixture consisting of propane and an inert diluent (CO_2), flowing vertically upward into a stationary air atmosphere, illustrates the Hilbert visualization frames shown in **Figures 7** and **8** (d = 3.2 mm). The digits below each frame indicate the sequence number of the frame, and the shooting frequency is 50 fps. Just as in the case of the use of Freon-22, the experiments are presented in flow regimes, in which a laminar-turbulent transition with a characteristic intermittency process began inside the tube.

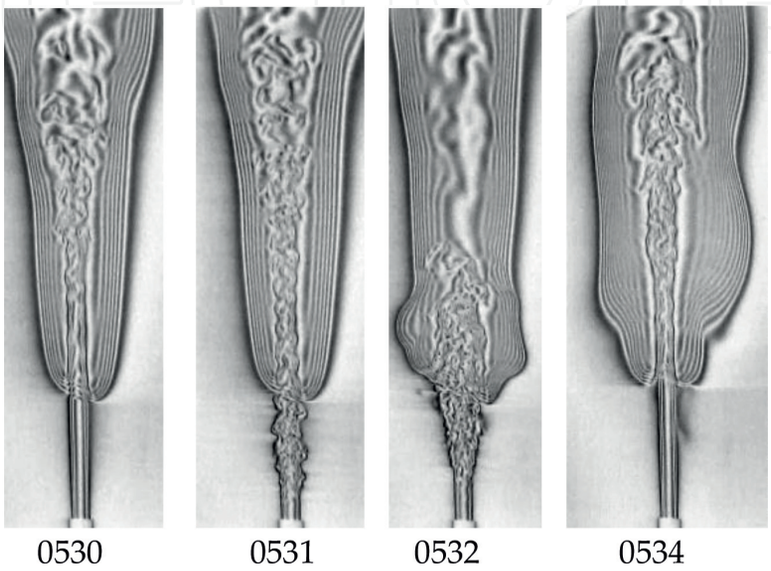

Figure 7. Laminar-lifted flame (Re = 2966, C_3H_8/CO_2, Y = 46).

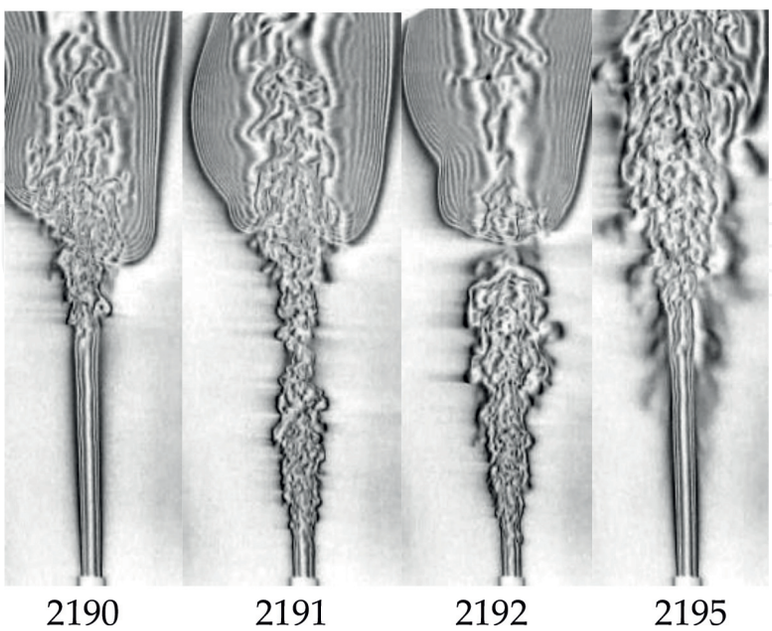

Figure 8. Flame extinction in the transient flow regime of the jet (Re = 2966, C_3H_8/CO_2, Y = 46) (see Video 3).

http://dx.doi.org/10.5772/intechopen.80610

In the attached mode of propane flame, the nature of the generation and dynamics of the propagation of the vortex structures along the flow do not undergo qualitative changes in comparison with the isothermal flow, although the influence of "puff-structures" on the low-frequency oscillations of the flame front is observed. When a puff appears in the observation zone, the wavelength of flicker oscillation increases by approximately 1.5–2 times. In the detached flame, the mutual influence of the vortex structures and the flame is much more pronounced. This may be caused by the known fact that in the vicinity of the flame front edge a local area of increased pressure is formed. **Figure 7** shows the effects of puff on a laminar-lifted flame. It can be seen that as the vortex structure passes along the jet, the leading edge of the flame undergoes significant changes in the spatial position and shape. In this case, low-frequency oscillations of the flame front leading edge are preserved, and combustion extinction is not observed. A completely different scenario of the flame-vortex interaction extinction is shown in **Figure 8**. The sequence of the Hilbert visualization frames in **Figure 8** illustrates the interaction of the vortex (frame 2191) with the lifted jet flame, which results in the extinction of the diffusion flame (frame 2195). The time interval between two adjacent frames (numbers) is 1/50 s.

Apparently, the impact of a large-scale perturbation led to the formation of a zone with a low-fuel content (frame 2192) in the near-axis area. These conditions are insufficient for combustion stabilization and led to a flame-off. So, vortex structure spontaneously arising in the tube affects the flame jet structure leading to its extinction.

It is known that the properties of hydrogen are very different from the thermal and chemical properties of hydrocarbons—H_2 has a low density and high values of the diffusion coefficient and, as a result, a high-flame propagation velocity. This inevitably affects the differences in the flame reaction to the appearance of vortex structures in the transient flow regime of the fuel in the tube. When hydrogen diluted with an inert gas is burned, the low-frequency flame flashes (flickering) can be suppressed almost completely (**Figure 9**).

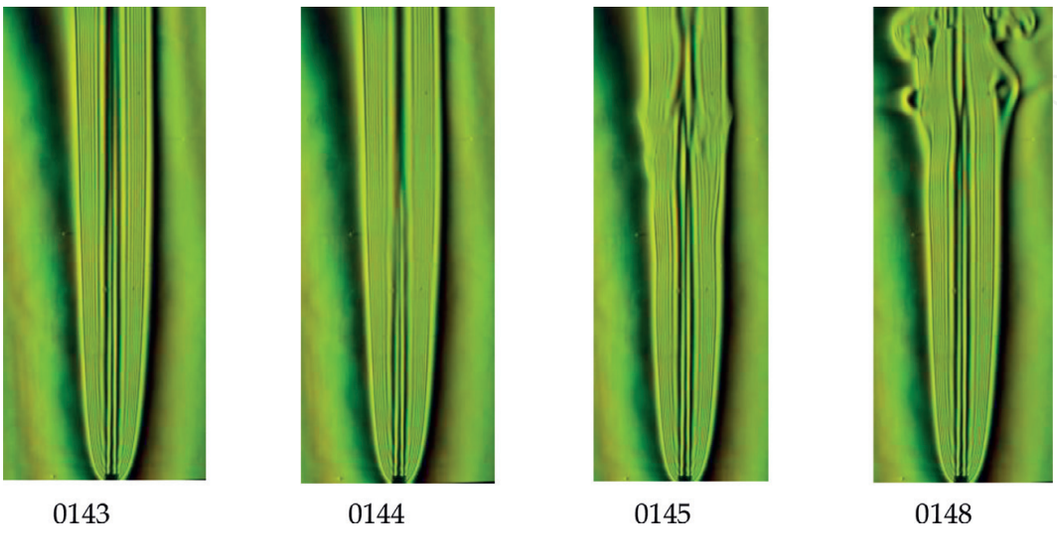

Figure 9. The attached H_2/CO_2 flame in the transient flow regime of the fuel jet (Re = 2870, Y = 90%) (see Video 4).

The flame can remain attached. The passage of vortex structures can be accompanied by the formation of "holes" in the flame—the dark areas shown in **Figure 9** (frame 0148), where combustion apparently, does not occur. Earlier, a similar phenomenon was discovered for the combustion of a methane jet at substantially higher Reynolds numbers [29].

6. The jet in a cross flow: a cold stream and a torch

Reacting jets are widely used in various types of burner devices. Jet flames have a simple, easily reproducible configuration and serve as an object of studies of the combustion dynamic fundamental principles, flame structure, and its stability both at combustion in still air and at interaction with air moving in different directions relative to the jet. One of the most important aspects of the problem is the flame extinction conditions, which determine the boundaries of the stable combustion and the range of admissible parameters for the stable operation of the burner device. Recent advances in the development of experimental diagnostics and numerical methods open new prospects in this field. For example, detailed experimental data on the flame structure for the combustion of a H_2/CO_2 mixture in a transverse flow, obtained using high-speed OH imaging and PLIF measurements, are presented in [30, 31], respectively.

One of the fundamental problems in the analysis of such processes is detecting and recording the flow parameters which ensure a stable combustion. Conditions for the jet flame extinction, i.e., the correlation of the cross flow velocity at which extinction occurs, fuel jet velocity, and other factors have been well established for hydrocarbon fuels. Recently, the conditions for stable burning of a jet flame of hydrogen fuel diluted with hydrocarbons (CO_2, CH_4, C_3H_8) in still air were investigated in [32]. The paper showed how additives of various gases affect the transition from the attached flame to the lifted one. In particular, it was noted that an increase in the proportion of hydrogen leads to a monotonic increase in the rate of the jet flame-off. In a number of studies, for example, in [33] it was noted that for detached and lifted flames, the extinction conditions differ significantly. In [34–36], semi-empirical methods were proposed to generalize the experimentally obtained data on the conditions of flame extinction in a cross

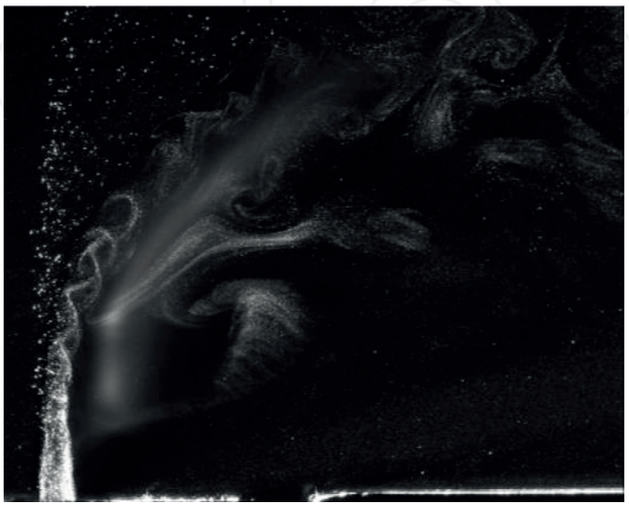

Figure 10. PIV visualization of the H_2/N_2 flame in air cross flow: d = 2 mm, H_2/N_2—Y = 36.7%, U_0 = 20 m/s, U_C = 8 m/s.

airflow. A review of physical mechanisms for jet flame stabilization is presented in [37]. Nevertheless, the parameters determining the hydrogen flame extinction for fuel mixtures with an inert diluent remain insufficiently investigated. To understand the mechanisms of turbulent flame stabilization, it is necessary to have detailed information on the structure and dynamics of heat-release regions in the flame and their interaction with the aerodynamics of the reacting flow. The topology of the heat-generating regions, even in the simplest configurations of the flow, may turn out to be nontrivial. Thus, for example, the PIV visualization of the combustion of a fuel jet, delivered through a hole in the wall into a transverse airflow, has revealed the formation of spiral vortices in the flame of a jet (**Figure 10**).

It should be noted that the structure of the flame will differ for hydrogen and hydrocarbon fuel. In addition, it is known that the initial temperature of the fuel mixture can significantly change the reacting flow characteristics. For example, the diffusion flame of preheated

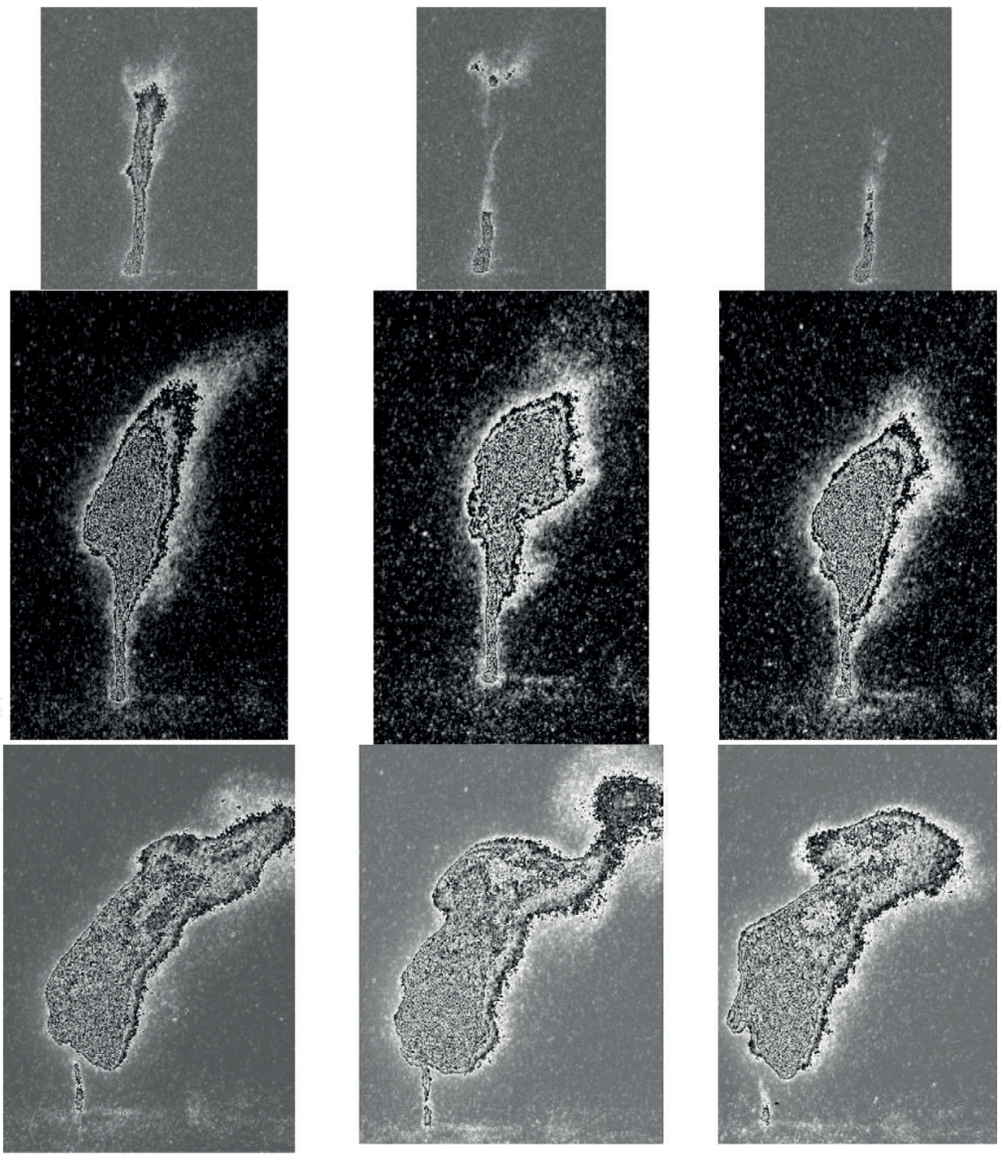

Figure 11. Chemiluminescence of OH radical in the wavelength range 306–308 nm with H_2/CO_2 jet combustion in air cross flows: d = 2 mm, U_0 = 60 m/s U_C = 8 m/s. Run 1, Y = 46%; Run 2, Y = 60%; and Run 3, Y = 70%.

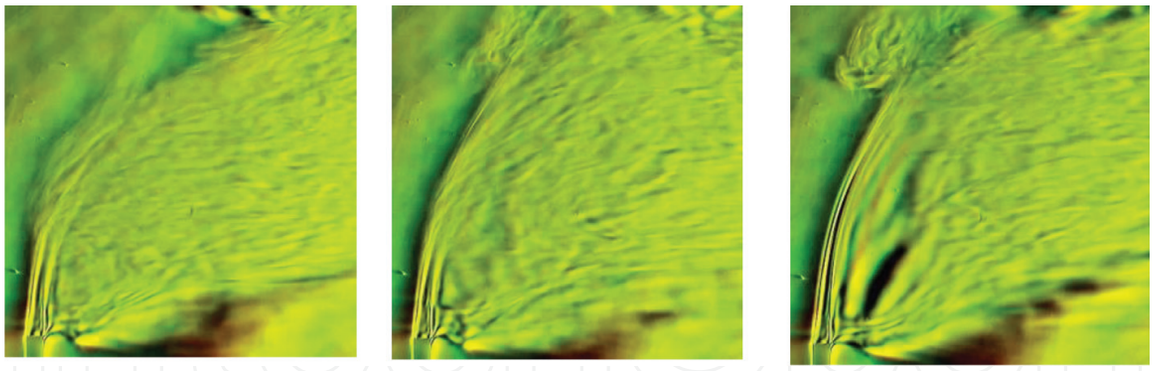

Figure 12. H_2/CO_2 flame jet in cross flow: d = 3.2 mm Re = 3476, Y = 39.4%, U_0 = 1.5 m/s.

propane is known to acquire the characteristic features of a hydrogen flame, in particular the formation of a thin luminous "filament" that connects the main flame body to the outlet of the fuel supply tube.

Photographing the chemiluminescence of the OH radical in the wavelength range 306–308 nm using the DiCAM-PRO ultraviolet camera is shown in **Figure 11**. The presented pictures were made in different, unrelated moments of time. Exposure time was chosen to provide the necessary level of illumination of the photosensitive matrix. In pre-extinction modes with maximum dilution of hydrogen by an inert gas (in mode Run 1), a torch body is not formed.

The flame-off at low hydrogen content (Run 1) achieved by gradual increase of the main flow velocity resembles the disappearance of a thin glowing filament. Under Run 2, all parts of the torch are observed until the moment of extinction. In Run 3, there are gaps in the body of the glowing filament. The change in the flame shape can be considered as a sign of a change in the mechanism of combustion stabilization.

New features are found for the diffusion flame in a cross flow at the instability regime in the jet source. As for combustion in still air, the intermittent character of the torch formation is revealed. In the laminar flow phase (**Figure 12** frame 360), an extended section of the longer-range jet is observed. When vortex structure appears, the flame topology changes dramatically: the flame length becomes shorter, and the curvature of the flame increases (frame 356). At a certain concentration of the diluent, the flame's body is divided into separate nonintersecting fragments.

7. Discussion and conclusion

In this chapter, hydrodynamics and combustion of a subsonic gas jet flowing out of the tube in the Reynolds number range 200–15,000 have been studied experimentally. The Reynolds numbers, characteristic of a laminar-turbulent transition in a pipe (both for cold-jet experiments and for combustion experiments), may differ due to the difference in the initial and boundary conditions in the pipe (velocity profile, turbulence level, non-isothermal conditions

on the wall) [8]. However, such fundamental processes as intermittence and formation of vortex structures (puff) are present in the initial section both in the "cold" and in the "hot" jet.

The average velocity and velocity ripples in the near field of a propane-butane jet without combustion have been measured under isothermal conditions. Two "laminar" and "transitional" regimes have been established, in which it is possible to control mixing and combustion in the jet instability region at low Reynolds numbers (Re < 4000). In the "laminar" mode, when there is no puff, the instability of the jet flow prevails [2, 3], which allows controlling vortex structures, for example, by acoustic impact. For the "transitional" regime, the mechanism of two-stage instability is caused by the formation of turbulent spots inside the tube [7, 8] and the generation of vortex structures in the jet [2, 3]. The velocity of the puff structure is consistent with the convective velocity of the jet on the axis. However, the acoustic precursor spreads before the disturbance, which significantly changes the instability wave in the jet-mixing layer.

Several new results have been obtained in combustion experiments. Visualization and measurements have shown that the vortex structures (puff) that form in the transient flow-out regime have a strong effect on the flame. First, the vortex structures affect the instability of the outer flame front in different ways: for the mixture (C_3H_8/CO_2, Y = 46%), low-frequency oscillations (F = 6–15 Hz) remain (see **Figure 6**), and for combustion (H_2/CO_2, Y = 90%), the phenomenon of flickering can be suppressed almost completely (see **Figure 8**). Secondly, a reduction in the fuel content for a fixed Re number can lead to a transition from the attached flame to the disconnected flame. Thus, when mixtures of C_3H_8 with CO_2 or He burn in a transient mode, the flame is detached from the edge of the tube. Thirdly, depending on the set of parameters Re and Y, both a disconnected laminar flame and a disconnected turbulent flame were observed. Under such conditions, a transition from turbulent combustion to laminar combustion and vice versa is possible. Fourthly, there is a range of parameters depending on d, Re, and Y, at which the disconnected turbulent flame can be disrupted. Our data show that extinction under such conditions is associated with the action of turbulent spots arising in the transient flow regime in the tube, on the region of jet disintegration (see **Figure 7**). In the case of the formation of a flame in a drifting stream, the intermittent nature of the flame is observed in the puff formation mode. Its length increases in the laminar flow phase and decreases in the turbulent phase (see **Figure 11**).

In addition, previously unknown data on the topology of the heat-release regions of the diffusion flare have been obtained. Thus, when H_2/CO_2 burns on the outer boundary of the attached flame (without a drift), the passage of puff can be accompanied by the formation of "holes" in the flame, i.e., dark areas in which combustion apparently does not occur (see **Figure 8**). The visualization of the combustion of a H_2/CO_2 fuel jet, fed through a hole in the wall into a transverse airflow, has revealed the formation of spiral vortices in the flame of the jet (see **Figure 8**). A characteristic feature of a hydrogen flame in a transverse flow is the formation of a thin luminous "filament" that connects the main body of the flame with the outlet of the fuel supply tube (see **Figure 10**).

The influence of the vortex structure on two very different classes of jet flames (free jet and cross flow jet) is considered. A comparative analysis of these two flows allows to show the scale of the effect on the flow prehistory in the supply tube.

Along with the traditional methods of controlling the processes of mixing and combustion, an approach using the instability development regimes for controlling diffusion combustion, both in the jet stream itself and inside the source of jet formation, seems promising.

Acknowledgements

This work was partially supported by the Russian Foundation for Basic Research (Grant No. 17-08-00958). Hot-wire anemometer measurements were funded by the Ministry of Science and Higher Education of the Russian Federation.

Nomenclature

U_0	mean velocity on the axis in the initial section of the jet (m/s)
U_m	bulk velocity (m/s)
U_x	mean velocity on the axis of the jet (m/s)
u	root-mean-square value of velocity pulsations (m/s)
Y	volumetric concentration of fuel (%)
d	tube diameter (mm)
L	length of turbulent spot (mm)
l	tube length (mm)
x	longitudinal coordinate counted from the beginning of the jet (m)
$Tu = u/U_0*100$	turbulence degree of flow (%)
Tu_0	initial level of flow pulsation decrease (%)
$Re = U_m d/\nu$	Reynolds number of the jet
ν	kinematic viscosity of gas (m^2/s)
τM	time (s)

Author details

Dubnishchev Yuri Nikolaevich*, Lemanov Vadim Vladimirovich, Lukashov Vladimir Vladimirovich, Arbuzov Vitali Anisiforovich and Sharov Konstantin Aleksandrovich

*Address all correspondence to: dubnistchev@itp.nsc.ru

Kutateladze Institute of Thermophysics, Novosibirsk, Russia

References

[1] Abramovich GN. Theory of Turbulent Jets. Cambridge, MA: MIT Press; 1963. 671 p

[2] Ho CM, Huerre P. Mint: Perturbed free shear layers. Annual Review of Fluid Mechanics. 1984;**16**:365-424. DOI: 10.1146/annurev.fl.16.010184.002053

[3] Michalke A. Mint: Survey on jet instability theory. Progress in Aerospace Sciences. 1984; **21**:159-199. DOI: 10.1016/0376-0421(84)90005-8

[4] Peters N. Turbulent Combustion. Cambridge: Cambridge University Press; 2000. 303 p. DOI: 10.1017/CBO9780511612701

[5] Takeno T, Kotani Y. Mint: Transition and structure of turbulent jet diffusion flames. Progress in Astronautics and Aeronautics. 1978;**58**:19-35. DOI: 10.1016/S0082-0784(06) 80744-7

[6] Takahashi F, Mizomoto M, Ikai S. Mint: Transition from laminar to turbulent free jet diffusion flame. Combustion and Flame. 1982;**48**:85-95. DOI: 10.1016/0010-2180(82) 90117-1

[7] Lemanov VV, Lukashov VV, Abdrakhmanov R, Arbuzov VA, Dubnishchev YN, Sharov KA. Mint: Regimes of unsteady exhaustion and diffusion combustion of a hydrocarbon fuel jet. Combustion, Explosion, and Shock Waves. 2018;**54**:121-127

[8] Mullin T. Mint: Experimental studies of transition to turbulence in a pipe. Annual Review of Fluid Mechanics. 2011;**42**:1-24. DOI: 10.1146/annurev-fluid-122109-160652

[9] Roquemore WM, Chen LD, Seaba JP, Tschen PS, Goss LP, Trump DD. Mint: Jet diffusion flame transition to turbulence. Physics of Fluids. 1987;**30**:2600-2600. DOI: 10.1063/ 1.4738813

[10] Katta VR, Goss LP, Roquemore WM. Mint: Numerical investigations of transitional H_2/N_2 jet diffusion flames. AIAA Journal. 1994;**32**:84-94. DOI: 10.2514/3.11954

[11] Smits A, Lim T. Flow Visualization. Techniques and Examples. London: Imperial College Press; 2000. 306 p

[12] Kleine H. Mint: Schlieren imaging and the real world. Journal of Visualization. 2013;**16**: 193-199. DOI: 10.1007/s12650-013-0169-y

[13] Dubnishchev Yu N, Rinkevichyus BS. Methods of the Laser Doppler Anemometry. Moscow: Nauka; 1982. [in Russian]

[14] Dubnishchev YN, Chugui YV, Kompenhans Y. Mint: Laser Doppler visualization of the velocity field with elimination of the influence of multiparticle scattering. Quantum Electronincs. 2009;**39**:962-966. DOI: 10.1070/QE2009v039n10ABEH014054

[15] Dubnishchev YN. Mint: Laser Doppler visualization of the fields of three-dimensional velocity vectors with the use of the minimum number of CCD cameras. Quantum Electronics. 2010;**40**:551-555. DOI: 10.1070/QE2010v040n06ABEH014296

[16] Dulin VM, Markovich DM, Tolkarev MP, Chikishev LM. Mint: Application of modern optical methods for detecting the spatial structure of turbulent flames. Optoelectronics, Instrumentation and Data Processing. 2012;**48**(3):235-243. DOI: 10.3103/S875669901203003X

[17] Raffel M, Willert CT, Wereley ST, Yu K. Particle Image Velocimetry. A Practical Guide. Berlin: Springer; 2007. 448 p

[18] Arbuzov VA, Arbuzov EV, Berdnikov VS, Bufetov NS, Dubnishchev YN, Shlapakova EO. Mint: Optical diagnostics of the structure and evolution lets in a high-viscosity fluid. Optoelectronics, Instrumentation and Data Processing. 2014;**50**(5):466-473. DOI: 103103/S8756699014050045

[19] Arbuzov VA, Arbuzov EV, Dvornikov NA, Dubnishchev YN, Nechaev VG, Shlapakova EO. Mint: Optical diagnostics of vortex ring–flame interaction. Optoelectronics, Instrumentation and Data Processing. 2016;**52**(2):66-72. DOI: 19.3103/S8756699016020084

[20] Arbuzov VA, Dvornikov NA, Dubnishchev YN, Nechaev VG, Novosyolova ON, Shlapakova EO. Mint: Hilbert diagnostics of vortex rings indused in air by a pressure pulse on a hole. International Journal of Spray and Spray and Combustion Dynamics. 2016, 2016;**8**(3):197-204. DOI: 10.1177/1756827716651763

[21] Arbuzov VA, Arbuzov EV, Dubnishchev Yu N, Sotnicov VV, Shibaev AA. Mint: Measurement of the velocity of Hilbert-visualized phase structures by the method of emulation of two-dimensional spatial filtering of their images. Optoelectronics, Instrumentation and Data Processing. 2016;**52**(2):66-72. DOI: 10.3103/S875669901606011X

[22] Reid RC, Prausnitz JM, Sherwood TK. The Properties of Gases and Liquids. New York: McGraw-Hill; 1977. p. 688

[23] Lemanov VV, Terekhov VI, Sharov KA, Shumeiko AA. Mint: An experimental study of submerged jets at low Reynolds numbers. Technical Physics Letters. 2013;**39**:421-423. DOI: 10.1134/S1063785013050064

[24] Aniskin VM, Lemanov VV, Maslov NA, Mukhin KA, Terekhov VI, Sharov KA. Mint: An experimental study of the flow of subsonic flat mini and micro air jets. Technical Physics Letters. 2015;**41**:46-49. DOI: 10.1134/S1063785015010034

[25] Lemanov VV, Terekhov VI, Sharov KA. Mint: Investigation of the flow in free and impinging air micro- and macrojets. Springer Proceedings in Physics. 2016;**185**:29-35. DOI: 10.1007/978-3-319-30602-5_4

[26] Hallberg MP, Strykowski PJ. Mint: On the universality of global modes in low-density axisymmetric jets. Journal of Fluid Mechanics. 2006;**569**:493-507. DOI: 10.1017/S0022112006002357

[27] Nikitin NV, Pimanov VO. Mint: Numerical study of localized turbulent structures in a pipe. Fluid Dynamics. 2015;**50**:655-664. DOI: 10.1134/S0015462815050075

[28] Nikitin NV, Pimanov VO. Mint: Sustainment of oscillations in localized turbulent structures in pipes. Fluid Dynamics. 2018;**53**:65-73. DOI: 10.1134/S0015462818010111

[29] Lyons KM, Watson KA, Carter CD, Donbar JM. Mint: On flame holes and local extinction in lifted-jet diffusion flames. Combustion and Flame. 2005;**142**(3):308-313. DOI: 10.1016/j.combustflame.2005.04.006

[30] Steinberg AM, Sadanandan R, Dem C, Kutne P, Meier W. Mint: Structure and stabilization of hydrogen jet flames in cross-flows. Proceedings of the Combustion Institute. 2013;**34**: 1499-1507. DOI: 10.1016/j.proci.2012.06.026

[31] Sullivan R, Wilde D, David RDR, Seitzman JM, Lieuwen TC. Mint: Time-averaged characteristics of a reacting fuel jet in vitiated cross-flow. Combustion and Flame. 2014;**161**: 1792-1803. DOI: 10.1016/j.combustflame.2013.12.022

[32] Wu Y, Lu Y, Al-Rahbi IS, Kalghatgi GT. Mint: Prediction of the liftoff, blowout and blowoff stability limits for pure hydrogen and hydrogen/hydrocarbon mixture jet flames. International Journal of Hydrogen Energy. 2009;**34**:5940-5945. DOI: 10.1016/j.ijhydene.2009.01.084

[33] Menon R, Gollahalli SR. Mint: Combustion characteristics of interacting multiple jets in cross flow. Combustion Science and Technology. 1988;**60**:375-389. DOI: 10.1080/00102208808923994

[34] Kalghatgi GT. Mint: Blow-out stability of gaseous jet diffusion flames. Part I: In still air. Combustion Science and Technology. 1981;**26**:233-239. DOI: 10.1080/00102208108946964

[35] Kalghatgi GT. Mint: Blow-out stability of gaseous jet diffusion flames. Part II: Effect of cross wind. Combustion Science and Technology. 1981;**26**:241-244. DOI: 10.1080/00102208108946965

[36] Dahm WJA, Maymant AG. Mint: Blowout limits of turbulent jet diffusion flames for arbitrary source conditions. AIAA Journal. 1990;**28**:1157-1162. DOI: 10.2514/3.25186

[37] Moore NJ, McCraw JL, Lyons KM. Mint: Observations on jet-flame blowout. International Journal of Reacting Systems. 2008;**2008**:461059. DOI: 10.1155/2008/461059

IntechOpen